Chapter 3

The Simplest 2-D Walker

This chapter is a reproduction of a paper by Mariano Garcia, Anindya Chatterjee, Andy Ruina, and Michael Coleman entitled "The Simplest Walking Model: Stability, Complexity, and Scaling. It was published in the ASME Journal of Biomechanical Engineering Vol. 120, April 1998, pp. 281 − 288. Some additional figures and text have been added in Section 3.7.2. Sentences which refer to these figures, as well as this paragraph, are shown in italics to denote material which did not appear in the original text.

My role in this paper was as follows: I concocted the model and its equations, and did all of the simulation and data collection, including finding gait cycles and analyzing them. The stability results suggested the possibility of period-doubling, and Anindya Chatterjee prodded me to look for it. Anindya and I also observed the scaling results and he formulated an analytic approach which we then implemented together. While implementing the approach, I realized that the higher-period solutions of $z(\tau_0)$ (Equation 3.5) represented "multiple swinging" solutions which had been found previously (but not reported) by Mike Coleman in a slightly more

complicated numerical model. Andy Ruina added the observations on nonholonomic issues, the energy-based derivation of the scaling rule, and the dimensional power scaling law.

3.0.3 Abstract

We demonstrate that an irreducibly simple, uncontrolled, 2D, two-link model, vaguely resembling human legs, can walk down a shallow slope, powered only by gravity. This model is the simplest special case of the passive-dynamic models pioneered by McGeer (1990a). It has two rigid massless legs hinged at the hip, a point-mass at the hip, and infinitesimal point-masses at the feet. The feet have plastic (no-slip, no-bounce) collisions with the slope surface, except during forward swinging, when geometric interference (foot scuffing) is ignored. After nondimensionalizing the governing equations, the model has only one free parameter, the ramp slope γ. This model shows stable walking modes similar to more elaborate models, but allows some use of analytic methods to study its dynamics. The analytic calculations find initial conditions and stability estimates for period-one gait limit cycles. The model exhibits two period-one gait cycles, one of which is stable when $0 < \gamma < 0.015$ rad. With increasing γ, stable cycles of higher periods appear, and the walking-like motions apparently become chaotic through a sequence of period doublings. Scaling laws for the model predict that walking speed is proportional to stance angle, stance angle is proportional to $\gamma^{1/3}$, and that the gravitational power used is proportional to v^4 where v is the velocity along the slope.

3.1   Introduction

How much of coordination is purely mechanics? Human motion is controlled by the neuro-muscular system. But bipedal walking, an example of a basic human motion, might be largely understood as a passive mechanical process, as shown for part of a stride by Mochon and McMahon (1980). McGeer (1990a) demonstrated, by both computer simulation and physical-model construction, that some anthropomorphic legged mechanisms can exhibit stable, human-like walking on a range of shallow slopes with *no* actuation and *no* control (energy lost in friction and collisions is recovered from gravity). Unlike control-based models of animal locomotion, where the controller tries to force a motion on the system, McGeer's models' gait cycles (sequences of exactly-repeated steps) are inherent products of the models' dynamics for the given parameters.

McGeer's results with *passive dynamic walking* machines suggest that the mechanical parameters of the human body (e.g. lengths, mass distributions) have a greater effect on the existence and quality of gait than is generally recognized. That is, one needs to study mechanics, not just activation and control, to fully understand walking.

To get a better sense of the role of passive dynamics, it is interesting, following McGeer, to study simple, purely mechanical models. Here, we study what we believe is the simplest model that is capable of mimicking bipedal gait. This model is a limiting case of the straight-legged walker of McGeer (1990a), and also of the double-pendulum ("compass-gait") point-foot models being studied by Goswami et al. (1997). Our model has a special mass distribution that further simplifies the underlying mechanics and mathematics.

Inverted double pendulum models have previously been proposed as simple models of bipedal locomotion. Katoh and Mori (1984) used a controlled double-pendulum model to build a walking robot. Their controller was based on the idea of finding and operating at a stable limit cycle. Hurmuzlu and Moskowitz (1986) found that in a similar, controlled double-pendulum model, ground impacts were a major contributor to dynamic walking stability, presumably because of the sudden reduction of volume in phase space they cause.

Alexander (1995) reviews several cases where simple models give greater insight into human motion than more complicated models. In the spirit of Alexander, we study the simplest walker with the hope that it adds some insight into bipedal locomotion.

3.2   The Model

A cartoon of our point-foot model is shown in Figure 3.1. It has two rigid legs connected by a frictionless hinge at the hip. The only mass is at the hip and the feet. The hip mass M is much larger than the foot mass m ($M \gg m$) so that the motion of a swinging foot does not affect the motion of the hip. This linked mechanism moves on a rigid ramp of slope γ. When a foot hits the ground (ramp surface) at *heelstrike*, it has a plastic (no-slip, no-bounce) collision and its velocity jumps to zero. *We do not consider elastic rebound here.* That foot remains on the ground, acting like a hinge, until the swinging foot reaches heelstrike. During walking, only one foot is in contact with the ground at any time; double support occurs instantaneously. Our model is a simplified version of the 2D straight-legged walker with more general mass distribution of McGeer (1990a), which has round

feet, and of Goswami et al. (1996a) which, like ours, has point-feet. Our model is also closely related to Alexander's "minimal biped" Alexander (1995) which has strictly massless, and thus non-deterministic, swing legs. By adding miniscule feet, we make the minimal biped deterministic.

The model's motion is governed by the laws of classical rigid-body mechanics. Following McGeer, we make the non-physical assumption that the swing foot can briefly pass through the ramp surface when the stance leg is near vertical. This concession is made to avoid the inevitable scuffing problems of straight-legged walkers. In physical models, one can attempt to avoid foot-scuffing by adding some combination of complications such as powered ankles, as done by McGeer (1990a), passive knees, as done by McGeer (1990b) and Garcia et al. (1997), or side-to-side rocking, as done by various walking toys, for example those of Mahan (US Patent Nos. RE13696, 1007218), Fallis (US Patent No. 376588), and Coleman and Ruina (1998), or the hip-cam walker of Lattanzio et al. (1992).

3.3   The Walking Map

3.3.1   Outline of Procedure

The general procedure for the design and study of these models is based on interpreting a step as a Poincaré map, or, as McGeer termed it, a "stride function." Gait limit cycles are fixed points of this function. In this nonlinear-dynamics approach, one way to evaluate the stability of a gait cycle is to use the eigenvalues of the linearized map at the fixed point. Readers not familiar with this approach can refer to Appendix 3.7.1 for a summary of the necessary dynamics language.
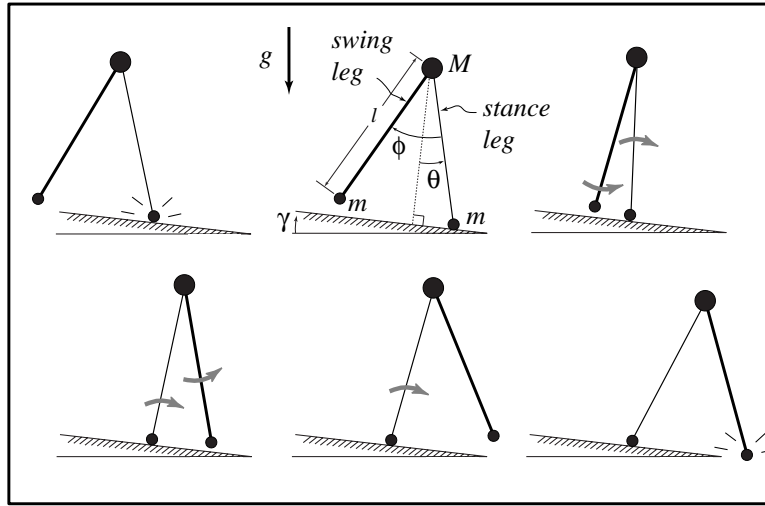
Figure 3.1: A typical passive walking step. The new stance leg (lighter line) has just made contact with the ramp in the upper left picture. The swing leg (heavier line) swings until the next heelstrike (bottom right picture). The top-center picture gives a description of the variables and parameters that we use. θ is the angle of the stance leg with respect to the slope normal. ϕ is the angle between the stance leg and the swing leg. M is the hip mass, and m is the foot mass. l is the leg length, γ is the ramp slope, and g is the acceleration due to gravity. Leg lines are drawn with different weights to match the plot of Figure 3.2.

3.3.2   Equations of Motion for the Swing Phase

The two coupled second-order differential equations of motion are given below for the swing phase of the motion, where $\beta = m/M$ and θ, ϕ are functions of time t. These two equations represent angular momentum balance about the foot (for the whole mechanism) and about the hip (for the swing leg), respectively.

$$\begin{bmatrix} 1 + 2\beta(1 - \cos\phi) & -\beta(1 - \cos\phi) \\ \beta(1 - \cos\phi) & -\beta \end{bmatrix} \begin{bmatrix} \ddot{\theta} \\ \ddot{\phi} \end{bmatrix} + \begin{bmatrix} -\beta\sin\phi(\dot{\phi}^2 - 2\dot{\theta}\dot{\phi}) \\ \beta\dot{\theta}^2\sin\phi \end{bmatrix}$$

$$+ \begin{bmatrix} (\beta g/l)[\sin(\theta - \phi - \gamma) - \sin(\theta - \gamma)] - g/l\sin(\theta - \gamma) \\ (\beta g/l)\sin(\theta - \phi - \gamma) \end{bmatrix} = \begin{bmatrix} 0 \\ 0 \end{bmatrix}$$

These are the equations of motion for a simple double pendulum. We will study the special case where the foot is much smaller than the body, because of its conceptual simplicity, and because human feet are small compared to the rest of the body. *In reality, of course, the functional contribution of the feet is more complicated than their role in this model.* Setting $\beta = 0$ (the limit as hip mass dominates foot mass) in the first equation of motion and dividing through by β in the second yields the two simpler equations which we use (Equation 3.1 and a trig identity are used to simplify Equation 3.2 also).

$$\ddot{\theta}(t) - \sin(\theta(t) - \gamma) = 0 \tag{3.1}$$

$$\ddot{\theta}(t) - \ddot{\phi}(t) + \dot{\theta}(t)^2\sin\phi(t) - \cos(\theta(t) - \gamma)\sin\phi(t) = 0 \tag{3.2}$$

In Equations 3.1 and 3.2, we have rescaled time by $\sqrt{l/g}$. Equation 3.1 describes an inverted simple pendulum (the stance leg) which is not affected by the motion of the

swing leg. Equation 3.2 describes the swing leg as a simple pendulum whose support (at the hip) moves through an arc. Note that there is only one free parameter in Equations 3.1 and 3.2: the ramp slope γ. (This parameter could also be removed from Equations 3.1 and 3.2 by replacing $\theta - \gamma$ with θ, but only at the expense of including γ in the heelstrike equations below.)

3.3.3   Transition Rule at Heelstrike Collision

Simulating the walker's motion consists of integrating equations of motion 3.1 and 3.2 and applying a transition rule when the swing foot hits the ground at heelstrike. The collision occurs when the geometric collision condition

$$\phi(t) - 2\theta(t) = 0 \tag{3.3}$$

is met. Equation 3.3 describes the values of ϕ and θ for which the swing foot is coincident with the ramp surface. We also impose the additional condition that the stance leg be sufficiently past vertical (Equation 3.3 is also true at least once when the legs are nearly parallel, but we ignore scuffing and let the swing leg swing through without collision).

At heelstrike, there is an impulse at the swing foot contact point. We assume, self-consistently, that the former stance leg (the new swing leg) has no impulsive reaction with the ground it is leaving. Neglecting non-impulsive forces at heelstrike, angular momentum is conserved through the collision for, a) the whole mechanism about the swing foot contact point, and b) the former stance leg (as it becomes the new swing leg) about the hip. The heelstrike angular momentum conservation relations give the following "jump" equation (for $\beta = 0$), where the "+" super-script means "just after heelstrike", and the "−" superscript means "just before

heelstrike".

$$
\begin{bmatrix} \theta \\ \dot\theta \\ \phi \\ \dot\phi \end{bmatrix}^{+} = \underbrace{\begin{bmatrix} -1 & 0 & 0 & 0 \\ 0 & \cos 2\theta & 0 & 0 \\ -2 & 0 & 0 & 0 \\ 0 & \cos 2\theta(1-\cos 2\theta) & 0 & 0 \end{bmatrix}}_{\mathbf{h}} \begin{bmatrix} \theta \\ \dot\theta \\ \phi \\ \dot\phi \end{bmatrix}^{-} \tag{3.4}
$$

Equation 3.4 also reflects a change of names for the two legs. The swing leg becomes the stance leg, and vice versa.

Our Poincaré section is at the start of a step, just after heelstrike. The Poincaré map $\mathbf{f}$ is from one section to the next section. That is, given the state of the system just after a heelstrike, the map $\mathbf{f}$ determines the state just after the next heelstrike, as defined by the solutions of governing ODEs (3.1) and (3.2) followed by the jump condition (3.4), denoted by $\mathbf{h}$. Note that the rank of $\mathbf{h}$ in Equation 3.4 is only 2, so the transition rule reduces this problem in 4D state space to a 2D map $\mathbf{f}$. The swing leg angle and rate after heelstrike, ϕ^{+} and $\dot\phi^{+}$, are determined by θ^{+} and $\dot\theta^{+}$. The physical reasons for this dimension-reduction are twofold: 1) The section is lower in dimension than the phase space; in this case θ and ϕ are coupled by the definition of the section (Equation 3.3). 2) Since the swing leg has only a point mass at the foot, it makes no contribution to the angular momentum of the system about the new contact point just before heelstrike; thus, the angular velocity of the swing leg before heelstrike does not affect the state just after heelstrike. Also, at the instant after heelstrike, the velocity of the newly swinging foot must point straight towards the hip (as a consequence of the transition rule). This dimension reduction

only depends on mass being concentrated at the hip and foot, not on the limit as $m/M \to 0$.

So, while the system can have four independent initial conditions, we need only to specify $\{\theta, \dot{\theta}\}^+$ at the start of walking step i to fully determine the subsequent motion at steps $i+1, i+2, ...$ so that $\{\theta, \dot{\theta}\}^+_{i+1} = \mathbf{f}(\{\theta, \dot{\theta}\}^+_i)$. This reduction of order was a primary motivation for concentrating mass at the hip and feet.

3.4 Analysis of the Model

3.4.1 Numerical and Analytic Tools

Our primary investigation tool is numerical simulation. We have checked the accuracy of our numerical results by verifying that calculated quantities (especially eigenvalues) do not change substantially when numerical tolerances are halved or doubled. Retaining numerical accuracy takes some care at very small slopes. Using a modified version of ODE45 in MATLAB, we specify a tolerance of 1e-12 in our numerical simulations. Collision configuration converges to machine accuracy. The Jacobian $\mathbf{J}$ of the linearized map (see Appendix 3.7.1) is calculated with perturbations of size 1e-6. So, we expect our numeric eigenvalues to be accurate to at least three decimal places (this is a worst-case estimate). Whether or not our numerical root-finding method locates all gait cycles (i.e. fixed points of $\mathbf{f}$) is an issue; see Appendix 3.7.1.

We also develop an asymptotic solution for the model's behavior at small slopes to understand how the dynamic variables and the step period scale with the slope. Asymptotic methods, which use the smallness of one or more parameters or variables, are useful in the regions where numerical methods are troublesome. Although

in practice, the analytic approach involves complicated symbolic manipulation at higher orders, the lowest-order approximation to the map gives an equation which governs the existence of gait cycles, as explained below and in Appendix 3.7.1. This equation from Appendix 3.7.1, and similar results from McGeer (1990a), give us some confidence that we have not missed any period-one gait cycles. Our analytic results also provide reasonably accurate initial guesses for our numerical gait-cycle searches (described below) which can then be extended to virtually any slope using path-following techniques. Agreement between the asymptotic-expansion approach and the numerical integration at small slopes gives some evidence of the validity of both techniques.

3.4.2 Finding Period-One Gait Cycles and Step Periods

To simulate the motion of the walker, we need to specify initial conditions $\{\theta, \dot{\theta}, \phi, \dot{\phi}\}^+$ at the start of the step. As mentioned previously, only $\{\theta, \dot{\theta}\}^+$ are independent, so to locate period-n gait cycles (fixed points of the map), we need to find initial conditions $\{\theta, \dot{\theta}\}^*$ such that after n steps, the system returns to the same initial conditions at the start of the nth step. We look for a step period that corresponds to a motion where the two legs pivot and swing, change angular velocities at heelstrike, and return to the same state after one or more heel strikes.

In the analytic search for period-one gait cycles we only deal with approximations of the first and second order. The main analytical result, derived as Equation 3.22 in Appendix 3.7.1, is that a period-one gait cycle is represented by zeros of the following function $z(\tau_0)$, where τ_0 is a first order approximation of the swing period τ. A similar function was derived by McGeer (1990a) in his analysis of a "synthetic wheel." *(See Appendix 3.7.2 for a plot of Equation 3.5.)*

$$z(\tau_0) = (1 + \exp \tau_0) \sin \tau_0 + 3(\exp \tau_0 - 1)(1 + \cos \tau_0) = 0 \qquad (3.5)$$

Following McGeer, we refer to the first two non-zero solutions to this equation as "short period" ($\tau_0 = \pi$) and "long period" ($\tau_0 \approx 3.8121$) gait cycles, respectively; these values are consistent with the numerical observations of McGeer (1990a) (our values are the limiting cases of the step period as $\gamma \to 0$). Since we can only solve for the long-period roots of Equation 3.5 numerically, we will express our analytic solutions in decimal form. More complicated models may have parameters in their version of Equation 3.5, and thus even the existence of gait cycles for other models may depend on parameter values. Note that to lowest order (in γ), the step period is constant, for small γ. That is, the step period τ does not change substantially with γ.

There are, in fact, infinitely many solution pairs to Equation 3.5 at $2n\pi + \tau_0, n = 1, 2 \ldots$. These larger-period roots of Equation 3.5 are probably not of much practical interest in studies of sober walking, since they correspond to multiple oscillations of the swing leg between heelstrikes *(see Appendix 3.7.2)*. Because we are only interested in reasonably anthropomorphic gaits (within the limitations of our model), we will restrict our attention to solutions which have $\tau_0 < 2\pi$.

3.4.3 Gait Cycle Stability

Once we find a gait cycle (specifically, a period-one gait cycle), we would like to characterize it as stable or unstable. The eigenvalues of the Jacobian **J** of the step-to-step map **f** govern the stability of the cycle. If all eigenvalues are within the unit circle, then the gait cycle is (asymptotically) stable. If one or more eigenvalues are

outside the unit circle, then the gait is unstable.

In the numerical approach, we find the Jacobian by perturbing the initial conditions in a small neighborhood of the fixed point. We then numerically calculate the eigenvalues for that Jacobian. We also used an analytic procedure to find an asymptotic approximation to period-one gait cycle eigenvalues, retaining terms up to $\mathcal{O}(\gamma^{2/3})$. This procedure is described by Coleman et al. (1997) in their analysis of a rimless spoked wheel; a brief summary is given in Appendix 3.7.1.

3.5 Results and Discussion

3.5.1 Typical Period-One Gait Cycles

We can find stable period-one gait cycles for slopes of $0 < \gamma < 0.0151$. A typical plot of θ and ϕ over one step is shown in Figure 3.2 for $\gamma = 0.009$.

Figure 3.3 shows a comparison between analytically-approximated (to $\mathcal{O}(\gamma)$) and numerically-found stance angles at the short and long period-one gaits, plotted as a function of γ. We expect, and find, that for this model, the fixed point must approach the inverted static solution as $\gamma \to 0$. The key scaling result, verified by numerical and analytical approaches, is that (to first order in $\gamma^{1/3}$) at a fixed point, the stance angle θ is proportional to the one-third power of the slope γ, and that the step period is approximately constant.

$$\theta^* \propto \gamma^{1/3} \tag{3.6}$$
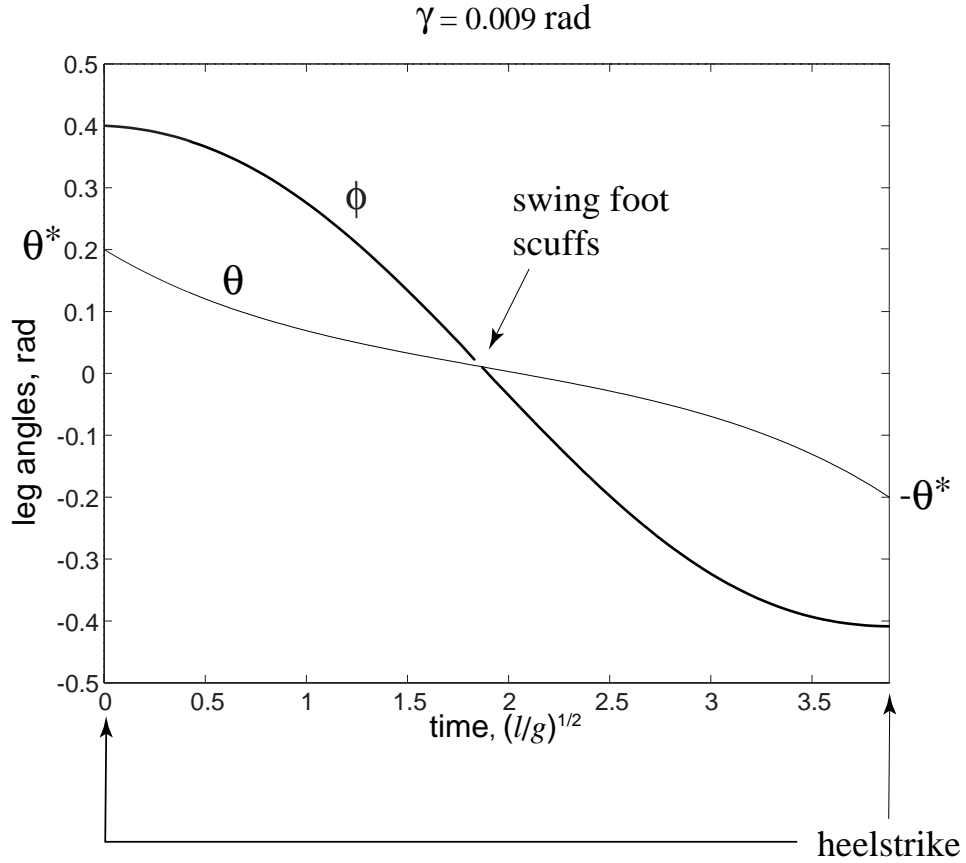
$$\tau^* \approx \tau_0 \tag{3.7}$$

Figure 3.2: Leg angles versus time over one step at a long-period gait cycle. At a gait cycle, heelstrike returns the system to its initial conditions. A perturbation analysis (Appendix 3.7.1) predicts $\theta^* \approx C_1 \gamma^{1/3} + C_2 \gamma$, where θ^* is the stance angle at a fixed point. The first term of the perturbation solution also predicts that $\dot{\phi} = 0$ just before and after heelstrike, and that the graph should have the time reversal symmetry (the graph looks the same when rotated 180 degrees).

This scaling result can also be argued as follows. The period of motion τ is approximately independent of γ, for small γ. Speeds thus scale with the stance angle θ^*. The angle by which the hip mass is deflected at heelstrike is $2\theta^*$. Angular momentum balance results in a heelstrike energy loss proportional to $\theta^{*2}(1 - \cos^2(\theta^*))$. Expanding $\cos(\theta^*)$ gives an energy loss per step proportional to θ^{*4}. The available gravitational potential energy per step is proportional to $\gamma\,\theta^*$. Equating available potential energy with lost kinetic energy yields $\gamma \propto \theta^{*3}$, or $\theta^* \propto \gamma^{1/3}$. Similar arguments are made by Alexander (1991, 1995).
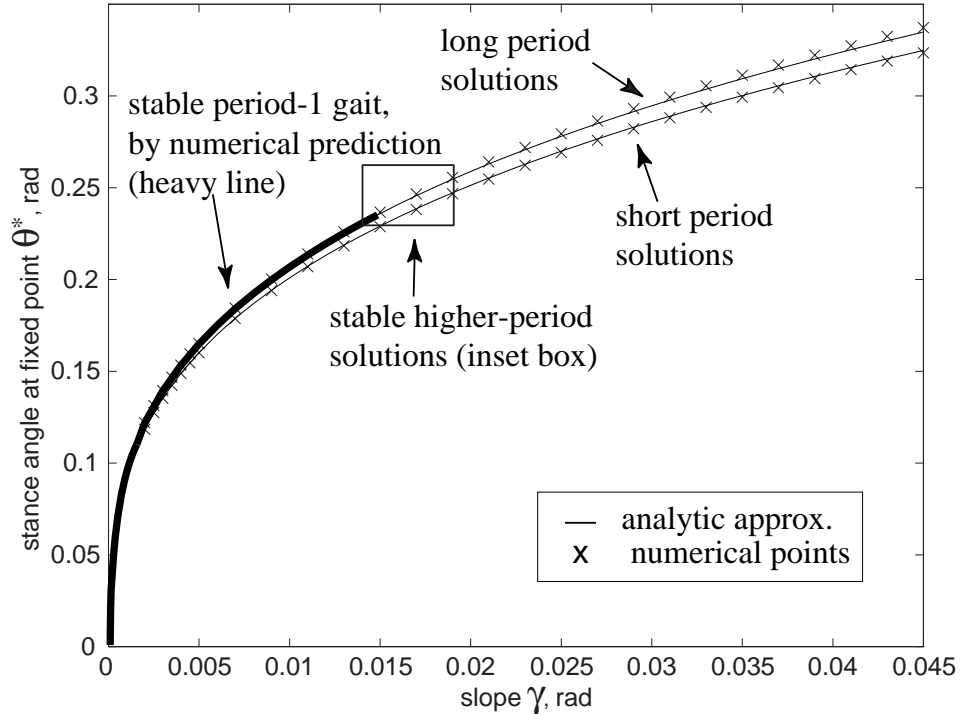

Figure 3.3: Numerical vs. analytic predictions for point-foot stance angle at fixed point as a function of slope. The short-period analytic solution is $\theta^* \approx 0.943976\gamma^{1/3} - 0.264561\gamma$. The long-period analytic solution is $\theta^* \approx 0.970956\gamma^{1/3} - 0.270837\gamma$, where θ^* is the stance angle at a fixed point. The inset box is shown expanded in Figure 3.6.

A careful numerical analysis predicts a region of stable period-one gait for slopes less than about $\gamma = 0.0151$. The analytic approach is inaccurate in estimating the critical slope as about 0.024. In contrast, the agreement between numerical and perturbation-analysis approaches is much better for the short-period gait. Analytic and numerical eigenvalue estimates are shown in Figure 3.4.

Presumably, a higher-order perturbation analysis would yield results that matched the numerics for both gaits more closely at higher slopes. Note that the eigenvalues of the long-period gait merge and split within the range of slopes studied; this appears to adversely affect the accuracy of the analytic eigenvalue estimates.
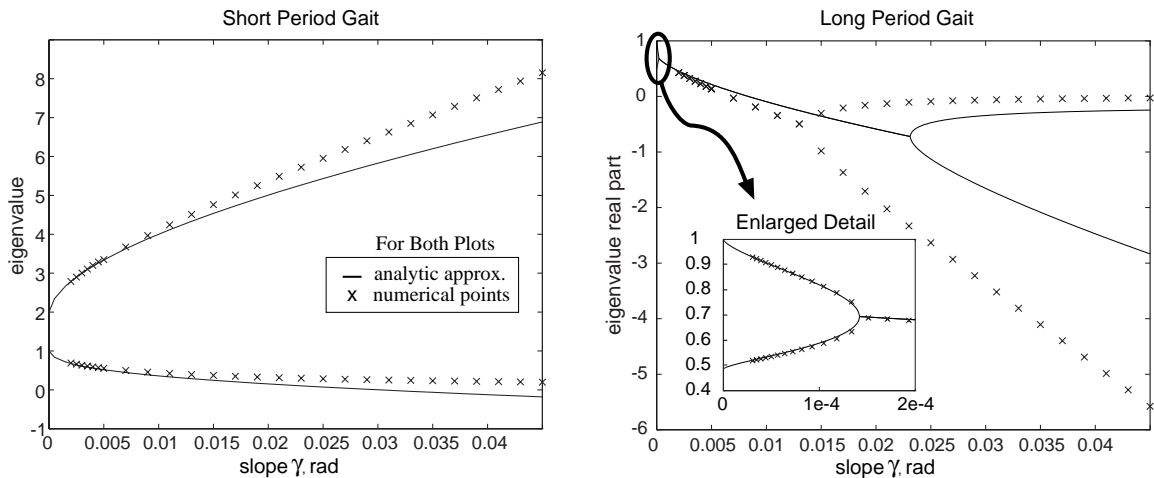

Figure 3.4: Comparison of analytic and numerical stability predictions for long and short period-one gait. The inset shows an expanded view of the numerical verification of the analytically-predicted split at $\gamma \approx 0.00014$ (upper left corner) for the long-period gait.

See Appendix 3.7.2 for a comparison of analytic predictions and numeric results of step periods at varying slopes.

3.5.2   Passive Dynamic Limping

Note the region of stable period-one gait in Figure 3.3; this motion bifurcates into a stable period-two gait as the period-one eigenvalue passes through -1 (the other eigenvalue is small and seems to have little effect on the walking motions). This "limping" bifurcation was also found independently by Goswami et al. (1996a) for a similar model.

A plot of one of these limping (period-two) solutions is shown in Figure 3.5. Note that limping gaits arise here from symmetric legs. This suggests, perhaps, that limping is a readily available natural mode of motion in human legs, even when they have symmetric mass distribution. *Pain in one leg could be alleviated by a switch in control strategy, from operating at a period-one cycle to operating at a period-two cycle, to minimize loading of the afflicted leg.* Also, even slight asymmetry in otherwise symmetric legs would result in the loss of normal (period-1) gait and might introduce unexpectedly severe limping (period-2) gait.

3.5.3   Period Doubling and Passive Dynamic Staggering

As γ is varied from 0.017 to 0.019, the stable 2-cycle bifurcates into a stable 4-cycle, and so on until the stable attractor appears chaotic. Some period doublings were also discovered independently in a slightly more complicated model by Thuilot et al. (1997) and Goswami et al. (1996b). This "period doubling route to chaos" is shown expanded in Figure 3.6. We did not perform any formal checks of this "chaos", except to observe that ratio of the distances between successive bifurcation values on the slope axis decreased roughly as follows: $5.9, 5.2, 4.6, \ldots$. (As discovered by Feigenbaum, the sequence of ratios is expected to converge to $4.669\ldots$
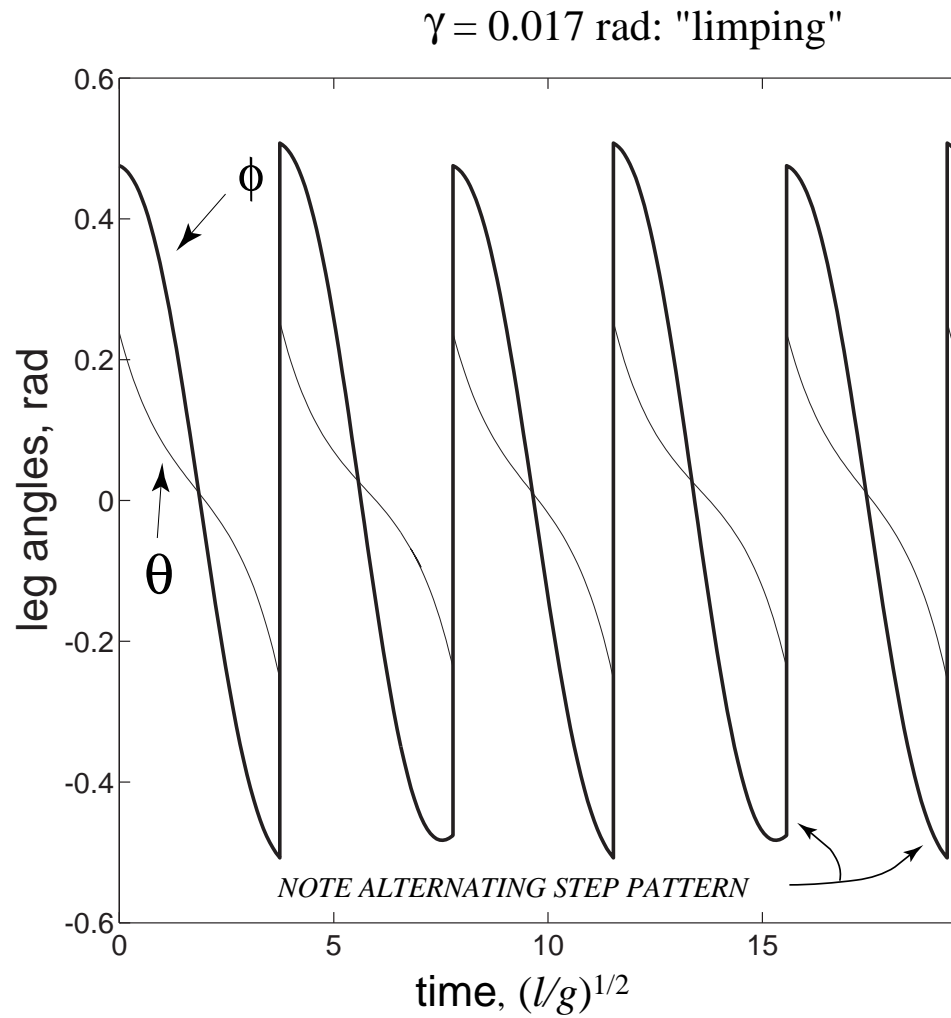
Figure 3.5: Several walker steps during a limping (period-two) gait. The walker's legs are symmetric, but the gait is not.

(Strogatz, 1995).) At slopes higher than $\gamma = 0.019$, the walker falls down; we could no longer find persistent walking motions. The box on Figure 3.3 shows the region where stable gaits of higher order appear. *Recently, Howell and Baillieul (1998) discovered a stable period-three gait for this model at a slope of $\gamma \approx 0.0125$.*
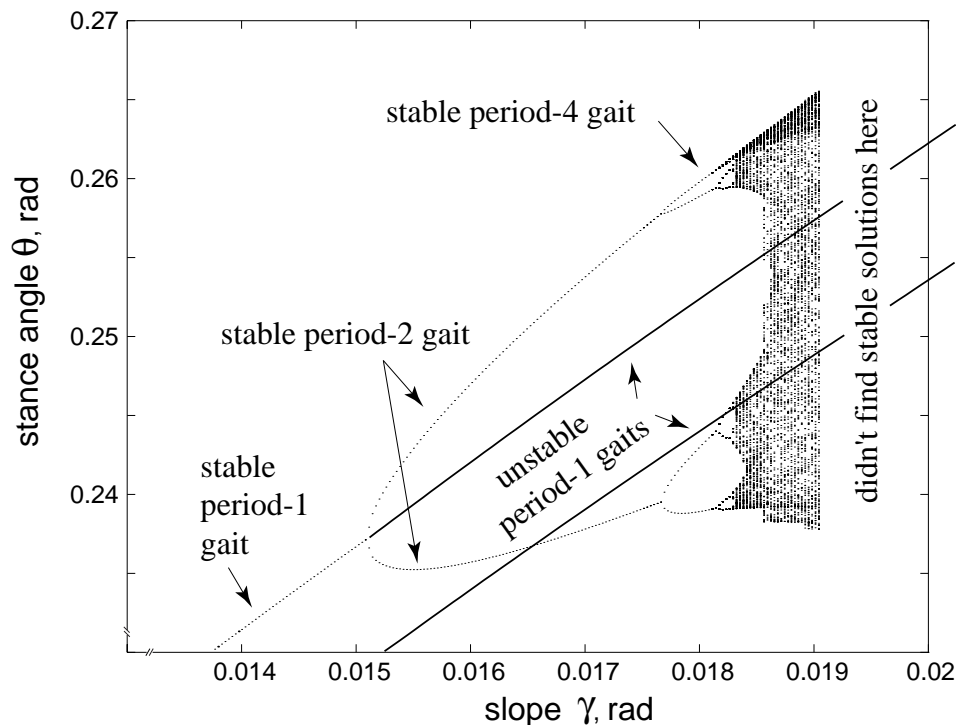
Figure 3.6: Period doubling of stable walking motions, inset from Figure 3.3. Unstable period-one cycles are shown for reference. Note that the line weights are opposite to the usual convention; dotted lines represent stable cycles while solid lines represent unstable ones. No persistent walking was found at slopes much steeper than 0.019 radians.

A plot of the chaotic attractor is shown in Figure 3.7 for $\gamma = 0.0189$. In this Poincaré section, each point represents the state of the system at the start of a step. The attractor evolves from gait cycles of increasingly higher period. (Following Goswami et al. (1996b) and Thuilot et al. (1997), and using 30,000 points, we

estimated the attractor's box-counting dimension (see e.g., Strogatz, 1995) to be about 1.25.)

The chaotic attractor of the walking mechanism brings up some interesting ideas. One usually thinks of periodic motions as being somehow more desirable and beneficial, but in fact the primary objectives in walking are usually to move quickly, efficiently, and not to fall down. Simple numerical experiments seem to imply that the basin of attraction for stable chaotic walking is, in some ways, bigger than the basins of the periodic fixed points, and therefore the chaotic walking motion might be more robust. It also may prove useful, if control is added, to keep the system in a chaotic region where many different step length combinations are readily available for the mechanism.

See Appendix 3.7.2 for figures of the return map and the evolution of the attractor, along with an inset of the attractor.

3.5.4 Energetic Cost of Locomotion

The simplest measure of passive walking efficiency is the minimum walking slope. If the walker could walk on level ground, it would be perfectly efficient, since it would require no energy for locomotion (energy loss per step $= 2Mgl \sin\gamma \sin\theta_s t$). For the point-foot walker, the stable gait cycles persist as the slope approaches level, although the gait velocity for these solutions also vanishes. In *some* sense, the dynamic solution approaches the static, parallel-leg solution as the ramp becomes flat. If the hip-mass were offset fore-aft from the legs, the gait cycles would approach a static solution at some non-zero slope which depended on this offset, and "near-perfectly efficient" walking would not be possible. So, for this model, and presumably for more complicated models, the existence of near-perfectly efficient
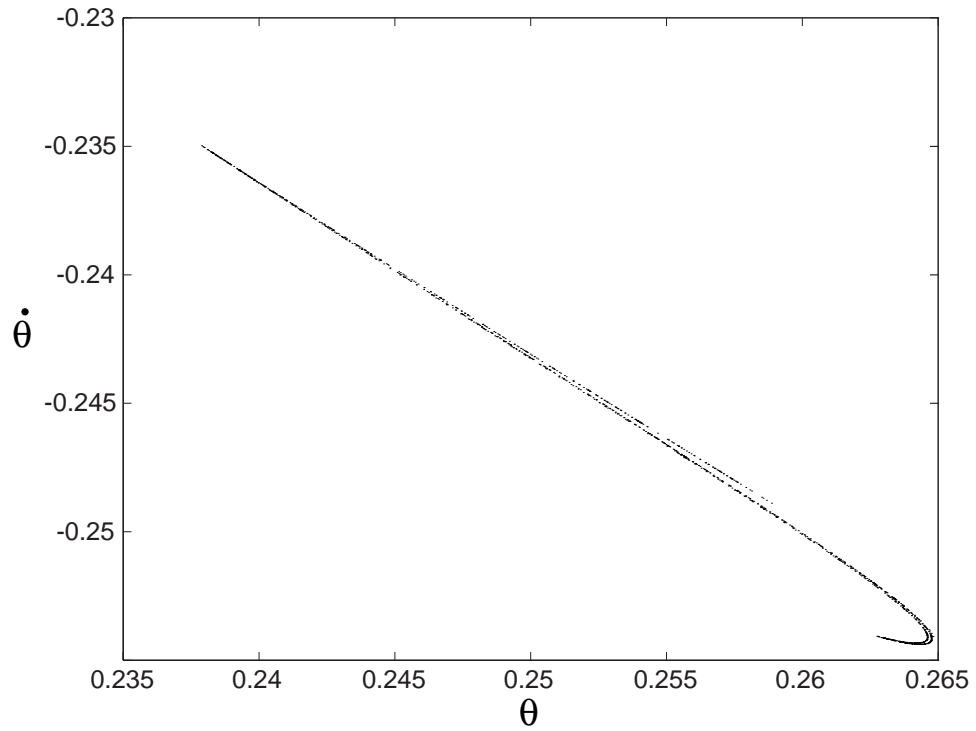
Figure 3.7: Poincaré section during chaotic walking motions, $\gamma = 0.0189$. Using 30,000 points, we calculate the box-counting dimension of the attractor to be about 1.25.

gait depends on the details of the mass distribution.

If we use the first-order scaling laws (Equations 3.6 and 3.7), expanding and retaining appropriate terms to re-dimensionalize the result, we find that the power used in locomotion for this model is approximately

$$P = Mgv\sin\gamma \approx \frac{\tau_0^3 Mv^4}{8\Theta_0(0)^3 l^{3/2}g^{1/2}} = C\frac{Mv^4}{l^{3/2}g^{1/2}} \tag{3.8}$$

where M is the mass of the walker, g is the acceleration due to gravity, v is the velocity down the slope, l is the leg length, τ_0 is the approximate non-dimensional step period, and $\Theta_0(0)$, which is about 1, is the first-order constant in the series expansion for θ (see Appendix 3.7.1). For the short period gait, $C \approx \pi^3/8 \approx 3.8758$, and for the long-period gait, $C \approx 3.8121^3/8 \approx 6.9247$.

For a 50 kg, 1m legged person walking at one meter per second this predicts a somewhat high 60 watts and 110 watts for the short and long period gaits, respectively. The power required for this model to walk is a strong function of velocity and decreases with increasing g. This scaling rule (3.8) follows from the scaling rules in Alexander (1995) and Alexander (1991) if we further assume that his minimal biped has a period independent of amplitude.

The short-period gait, although unstable, is significantly more efficient than the long-period gait, for a given velocity (this would not necessarily be true if the model was changed to have non-negligible foot masses, since there would also be a contribution to energy losses from foot collisions).

3.5.5 Energy Dissipation and Stability

As is well known in dynamical systems theory, conservative holonomic (i.e. Hamiltonian) systems cannot have asymptotic stability, since volume is conserved in their phase spaces. This walker is not conservative, since energy is lost at every heelstrike. As discussed indirectly in Hurmuzlu and Moskowitz (1986), these dissipative collisions allow the possibility of asymptotic stability, since at collisions, some regions in the model's phase space not only drop in volume, but also in dimension (the rank of $\mathbf{h}$ is 2, not 3). But, there are also slopes for which dissipation exists and yet the walking motions are unstable, so dissipation by itself does not guarantee stability. Also, as we noted, the motions retain some slight stability, in that one eigenvalue approaches 1 from below, as the collision losses vanish (when the slope γ and the stance angle θ^* go to zero).

Also, some smooth, conservative, *nonholonomic* systems can have asymptotically-stable, steady motions, as discussed by Bloch et al. (1996) and Zenkov et al. (1997). Bicycles (Hand, 1988), and skateboards (Hubbard, 1979) are two examples. A direct comparison between our walking mechanism and these other systems cannot be made, since walking is piecewise holonomic and dissipative. However, bicycles, skateboards, and other nonholonomic gadgets share the following feature with walkers: the dimension of the accessible configuration space (for the walker, one translation plus two angles) is larger than the dimension of the instantaneously accessible velocity space (for the walker, two angular velocities). For smooth systems, this trait is equivalent to the usual definition of non-holonomicity in Goldstein (1980). Coleman et al. (1997) have shown another piecewise holonomic, but globally non-holonomic system (similar to ours) that may depend on its nonholonomicity for stability. The role of this type of nonholonomic behavior in the asymptotic stability

of dissipative, piecewise holonomic systems with intermittent contact, is not well-understood at present. See Ruina (1998) for another example and more discussion.

3.6 Discussion and Conclusion

Most good controllers take advantage of the natural dynamics of their respective systems, and the human nervous system is probably no exception to this rule. Human locomotion is a controlled and complicated process, but to learn more about human locomotion, it is interesting to observe how the simplest, uncontrolled models can exhibit an array of complex and chaotic motions, both stable and unstable. The dynamics of these uncontrolled systems are based on mass distribution and length characteristics rather than on control strategy. Their stability mechanisms may also depend to some extent on their nonholonomic nature.

We have shown that the simplest uncontrolled walking model can walk stably. It can also limp and stagger. Its power consumption is proportional to the fourth power of its velocity. These results buttress the claim that passive-dynamic models might be a natural starting point for understanding some aspects of animal (including human) motion. It may be that many animal motions are largely natural or quasi-passive and not heavily controlled. In the context of walking, such results might be useful to those studying the active control aspects of walking, to those trying to design anthropomorphic robots, and to those trying to improve prosthetic devices and rehabilitation procedures.

3.7 Simplest Walker Appendices

3.7.1 Appendices Appearing In The Original Paper

Mathematical Tools and Dynamics Language

A *step* can be thought of as an operator $\mathbf{f}(\mathbf{q})$, the "stride function," which takes as input the list of values of the various angles and rates (the state variable vector $\mathbf{q}$) at a definite point in the motion (just after ground-collision for our purposes), and returns the values of $\mathbf{q}$ after the next ground-collision. In the language of dynamical systems, McGeer's stride function is a Poincaré map. Many questions about the dynamics of a given walking model are then reduced to questions about the function $\mathbf{f}(\mathbf{q})$ (also called a "map" or "mapping").

The function $\mathbf{f}(\mathbf{q})$ is found by first constructing governing differential equations and jump conditions for the model. The equations must then be solved, analytically if possible, but most often numerically. The solution of the equations for a period of time corresponding to one step, for a given set of initial conditions, yields one evaluation of $\mathbf{f}(\mathbf{q})$.

A simple (period-one) *gait cycle*, if it exists, corresponds to a set of initial values for the angles and rates which lead back to the same angles and rates after one step. This $\mathbf{q}^*$ is a "fixed point" of the function $\mathbf{f}(\mathbf{q})$, i.e., $\mathbf{f}(\mathbf{q}^*) = \mathbf{q}^*$. This corresponds to a zero, or root, of the function $\mathbf{g}(\mathbf{q}) \equiv \mathbf{f}(\mathbf{q}) - \mathbf{q}$. A *period-two* gait cycle returns the same variable values after *two* steps: $\mathbf{f}(\mathbf{f}(\mathbf{q}^*)) = \mathbf{q}^*$, and so on. (Of course, a period-one cycle is also a period-two cycle, since $\mathbf{f}(\mathbf{q}^*) = \mathbf{q}^*$ implies that $\mathbf{f}(\mathbf{f}(\mathbf{q}^*)) = \mathbf{q}^*$.) The term "gait cycle" by itself usually implies a period-one gait cycle.

All of these gait cycles are periodic walking solutions, although other non-periodic walking solutions exist. Longer-term numerical simulations are used to

analyze these cases: to see how the walker approaches a gait cycle, to map regions in state-space which approach gait cycles ("basins of attraction"), or to see how the walker falls down.

Periodic gait cycles are found numerically by searching, using analytic estimates as guesses for initial conditions, with a multidimensional Newton-Raphson method, for $\mathbf{q}^*$ such that $\mathbf{g}(\mathbf{q}^*) = \mathbf{0}$ (the function $\mathbf{g}$ is constructed numerically). Once found, the linearized stability of these cycles can be determined by finding the eigenvalues of the Jacobian $\mathbf{J}$ of the map $\mathbf{f}$. Here $\mathbf{J}$ is the matrix $\partial \mathbf{f}/\partial \mathbf{q}$ with components $\partial f_i/\partial q_j$. $\mathbf{J}$ is constructed by numerically evaluating $\mathbf{f}$ a number of times in a small neighborhood of $\mathbf{q}^*$ (i.e. numerically perturbing each component of $\mathbf{q}$).

Small perturbations $\hat{\mathbf{q}}$ to the limit cycle state vector $\mathbf{q}^*$ at the start of a step will grow or decay from the kth step to the $(k+1)^{th}$ step approximately according to $\hat{\mathbf{q}}^{k+1} \approx \mathbf{J}\hat{\mathbf{q}}^k$. If the map Jacobian $\mathbf{J}$ has all of its eigenvalues inside the unit circle, all sufficiently small perturbations will decay to $\mathbf{0}$, the system will return to its limit cycle, and the cycle is asymptotically stable. If the Jacobian has any eigenvalues outside the unit circle, any perturbation along the corresponding eigenvector will grow in time, steadily driving the system off the limit cycle, so the cycle is unstable. If an eigenvalue has magnitude of one, then the cycle is neutrally stable for infinitesimal perturbations along the corresponding eigenvector and such perturbations will neither shrink nor grow (to first order).

A given mechanism can have different solutions, with different stability, depending on its initial state vector and the slope of the ramp that it is on. Design of a successful physical passive-dynamic walker depends on both finding fixed points of $\mathbf{f}$ and having the eigenvalues of the Jacobian $\mathbf{J}$ all inside the unit circle on the complex plane.

Asymptotic Solution

For this and more complex models walking motions of interest are at relatively small slopes, so explicitly assuming small slopes seems to be a reasonable approach. We employ a perturbation method in order study walking cycles as $\gamma \to 0$. With numerical results as a guide, we define the scaling parameter ϵ and scaled variables Θ and Φ by

$$\gamma = \epsilon^3, \quad \theta(t) = \epsilon\Theta(t), \quad \dot{\theta}(t) = \epsilon\dot{\Theta}(t), \quad \phi(t) = \epsilon\Phi(t), \quad \dot{\phi}(t) = \epsilon\dot{\Phi}(t) \tag{3.9}$$

Substituting these into Equations 3.1 and 3.2 and expanding in a power series gives two governing equations with no order zero coefficient in ϵ, so we can divide both equations by ϵ. Since we are left with only even powers of ϵ, we can define δ as $\delta = \epsilon^2 = \gamma^{2/3}$ and after substituting, we are left, to $\mathcal{O}(\delta^2)$, with

$$\ddot{\Theta} - \Theta + \delta(1 + \frac{1}{6}\Theta^3) - \delta^2(\frac{1}{2}\Theta^2 + \frac{1}{120}\Theta^5) \approx 0 \tag{3.10}$$

$$\ddot{\Theta} - \Phi - \ddot{\Phi} + \delta(\dot{\Theta}^2\Phi + \frac{1}{2}\Theta^2\Phi + \frac{1}{6}\Phi^3) - \delta^2(\frac{1}{6}\Phi^3\dot{\Theta}^2 +$$
$$\Theta\Phi + \frac{1}{24}\Theta^4\Phi + \frac{1}{12}\Theta^2\Phi^3 + \frac{1}{120}\Phi^5) \approx 0. \tag{3.11}$$

where $\Theta \equiv \Theta(t), \Phi \equiv \Phi(t)$.

We assume power series solutions of the form

$$\Theta(t) = \Theta_0(t) + \delta\Theta_1(t) + \delta^2\Theta_2(t) + \dots \tag{3.12}$$

$$\Phi(t) = \Phi_0(t) + \delta\Phi_1(t) + \delta^2\Phi_2(t) + \dots \tag{3.13}$$

and initial conditions of the form

$$\Theta(0) = \Theta_0(0) + \delta\Theta_1(0) + \delta^2\Theta_2(0) + \dots \tag{3.14}$$

$$\dot{\Theta}(0) = \dot{\Theta}_0(0) + \delta\dot{\Theta}_1(0) + \delta^2\dot{\Theta}_2 + \dots \tag{3.15}$$

$$\Phi(0) = \Phi_0(0) + \delta\Phi_1(0) + \delta^2\Phi_2(0) + \dots \tag{3.16}$$

$$\dot{\Phi}(0) = \dot{\Phi}_0(0) + \delta\dot{\Phi}_1(0) + \delta^2\dot{\Phi}_2(0) + \dots \tag{3.17}$$

which are to be made consistent with the transition and collision conditions (3.4) to the appropriate order(s).

To zero-order in δ, the system motions (solutions to Equations 3.10, 3.11 and 3.4 with $\delta = 0$) are:

$$\Theta_0(t) = \frac{1}{2}[\Theta_0(0) + \dot{\Theta}_0(0)]\exp t + \frac{1}{2}[\Theta_0(0) - \dot{\Theta}_0(0)]\exp(-t) \tag{3.18}$$

$$\Phi_0(t) = \frac{1}{2}\Theta_0(t) - \frac{1}{2}\dot{\Theta}_0(0)\sin t + \frac{3}{2}\Theta_0(0)\cos t \tag{3.19}$$

Θ_0, Φ_0, and τ_0 are the first terms in the expansions of the state variables θ, ϕ, and the step period τ as functions of the slope γ.

$$\theta(t) \approx \Theta_0(t)\gamma^{1/3}, \quad \phi(t) \approx \Phi_0(t)\gamma^{1/3}, \quad \tau \approx \tau_0 \tag{3.20}$$

A fixed point (gait limit cycle) of the walking map requires that once the collision condition is met, heelstrike is about to occur, and the transition formula (eqn. 3.4) must produce the original initial conditions. Thus, we have three conditions for our zero-order ("linearized") solution: the double contact condition and the jump conditions for θ and $\dot{\theta}$. To first order, we can write these as follows, where τ_0 is the step period of the linearized system.

$$\Theta_0(0) = -\Theta_0(\tau_0), \quad \dot{\Theta}_0(0) = \dot{\Theta}_0(\tau_0), \quad \Phi_0(\tau_0) = 2\Theta_0(\tau_0). \qquad (3.21)$$

Substituting from the linearized system motions (Equations 3.18 and 3.19), we rearrange terms to get the following equations for τ_0 and $\dot{\Theta}_0$

$$z(\tau_0) = \cos(\tau_0/2) \cdot \{(1 + \exp\tau_0)\sin(\tau_0/2) + 3(\exp\tau_0 - 1)\cos(\tau_0/2)\} = 0 \quad (3.22)$$

$$\text{with} \qquad \dot{\Theta}_0(0) = \underbrace{\frac{1 + \exp\tau_0}{1 - \exp\tau_0}}_{\alpha} \Theta_0(0) \qquad (3.23)$$

Equation 3.22 is equivalent to Equation 3.5 in the text. Equation 3.22 has roots $\tau_0 = \pi, 3\pi, \ldots (2n+1)\pi$ associated with the cosine term and another set of roots associated with the $\{\}$ term that are $\tau_0 = 0, 3.812092, \ldots$ that can be found numerically. Each root of $z(\tau_0)$ corresponds to a unique solution for the period of a unique period-one gait cycle in the linearized (first order) model. The roots associated with the $\{\}$ term satisfy the symmetry conditions that $\Theta(\tau_0/2) = 0$ and $\Phi(\tau_0/2) = 0$, have $\dot{\Phi}(\tau_0) = 0$, and have no scuffing at heel-strike (to first order).

Note that $\Theta_0(0)$ and $\dot{\Theta}_0(0)$ cannot be found at this order, but only at the next order. In general, at order k in δ, we are able to find the step period coefficient τ_k, and one condition on the coefficients Θ_k and $\dot{\Theta}_k$. At the same time, we are able to solve for Θ_{k-1} and $\dot{\Theta}_{k-1}$. So, although the $O(\delta)$ equations are more complicated, the analysis is similar to the previous one. Because the equations become longer, however, we will omit some of the details. Using known solutions to the order zero equations, we first solve the $O(\delta)$ differential equations for $\Theta_1(t)$ and $\Phi_1(t)$, subject to initial conditions consistent with the jump conditions for θ and $\dot{\theta}$ (obtained

again by series expansion). $\Theta_1(0)$ and $\dot{\Theta}_1(0)$ are unknowns now. Together with the collision condition, this gives us three more equations in $O(\delta)$.

$$\dot{\Phi}_0(\tau_0)\tau_1 + \Phi_1(\tau_0) - 2\alpha\Theta_0(0)\tau_1 - 2\Theta_1(\tau_0) = 0 \tag{3.24}$$

$$\Theta_1(0) + \alpha\Theta_0(0)\tau_1 + \Theta_1(\tau_0) = 0 \tag{3.25}$$

$$\dot{\Theta}_1(0) + \Theta_0(0)\tau_1 - \dot{\Theta}_1(\tau_0) + 2\alpha\Theta_0{}^3(0) = 0 \tag{3.26}$$

Numerically evaluating this set of equations and solving for the unknowns $\{\Theta_1(0),$ $\dot{\Theta}_1(0), \tau_1\}$ results in a set of equations of the form

$$\mathbf{A} \begin{bmatrix} \Theta_1(0) \\ \dot{\Theta}_1(0) \\ \tau_1 \end{bmatrix} = \mathbf{b}_1 + \Theta_0^3(0)\mathbf{b}_2 \tag{3.27}$$

where the left-hand matrix $\mathbf{A}$ is singular. So, if a solution exists it must be true that $\mathbf{v}^T\mathbf{b}_1 + \mathbf{v}^T\mathbf{b}_2\Theta_0^3(0) = 0$ where $\mathbf{v}$ is the zero-eigenvalue eigenvector of $\mathbf{A}^T$ (Fredholm alternative). Solution is straightforward; we now have a value for $\Theta_0(0)$ at the gait cycle *in terms of* γ. In other words, we have a linear approximation to the values of the fixed point for small slopes. We can also solve for τ_1, since the null eigenvector of $\mathbf{A}$ has a zero in the τ_1 place. Lastly, we can derive the relationship $\dot{\Theta}_1(0) = \alpha\Theta_1(0) + c_1$, but, as expected, we need to go to the next-higher order to solve for $\Theta_1(0)$.

So, at small γ, we expect fixed point initial conditions to be, to $\mathcal{O}(\gamma)$,

$$\begin{bmatrix} \theta \\ \dot{\theta} \\ \phi \\ \dot{\phi} \end{bmatrix}^+ \approx \begin{bmatrix} \Theta_0(0)\gamma^{1/3} + \Theta_1(0)\gamma \\ \alpha\Theta_0(0)\gamma^{1/3} + (\alpha\Theta_1(0) + c_1)\gamma \\ 2\theta^+ \\ \dot{\theta}^+(1 - \cos 2\theta^+) \end{bmatrix} \tag{3.28}$$

and the swing period to be

$$\tau = \tau_0 + \tau_1\gamma^{2/3} + \tau_2\gamma^{4/3} + \mathcal{O}(\gamma^2) \qquad (3.29)$$

Table 3.1 summarizes our analytic results for the first two period-one fixed points of the walking map.

Table 3.1: Summary of analytic results for the first two period-one fixed points of the walking map for the simplest walker.

gait	τ_0	τ_1	τ_2	$\Theta_0(0)$	$\Theta_1(0)$	α	c_1
short	π	-0.90750	-4.56225	0.94398	-0.26456	-1.09033	0.86661
long	3.81209	1.57913	0.93202	0.97096	-0.27084	-1.04520	1.06290

Analytic Stability Approximation

Using our $O(\delta^2)$ approximation to the fixed point, we can also find an approximation to $\mathbf{J}$ in order to predict the stability of the system to $O(\delta)$ by expanding perturbations to the limit cycle in a similar way. We followed the procedure in Coleman et al. (1997) for an analysis of a 3D rimless wheel.

A brief summary of the procedure followed in Coleman et al. (1997) is as follows. Just after one collision, let's say we have a small perturbation to the limit cycle $\zeta\hat{\mathbf{q}}$. This perturbation evolves in time until, at the limit cycle period τ^*, it is $\zeta\hat{\mathbf{q}}^*$. However, heelstrike occurs at a slightly different time and at a slightly different configuration than the limit cycle value $\mathbf{q}^*$. These three effects (evolution of initial perturbation, change in step period, and change in collision configuration) can be described, for the purposes of linearized stability analysis, by the product of three matrices. The product of these is exactly equal to the Jacobian. Each matrix can

in turn be approximated by an asymptotic expansion in the small parameter δ. The product of these three matrices is exactly equal to the Jacobian **J**.

Using this procedure, we found approximate Jacobians for the long and short period gaits to be (to first order in δ):

$$\tau_0 = \pi : \quad \mathbf{J} \approx \begin{bmatrix} 7.29598 & 5.77437 \\ -5.77437 & -4.29598 \end{bmatrix} + \begin{bmatrix} 17.22975 & 17.86638 \\ 21.06968 & 12.08449 \end{bmatrix} \gamma^{2/3}$$

$$\tau_0 \approx 3.8121 : \quad \mathbf{J} \approx \begin{bmatrix} -5.07075 & -5.80820 \\ 5.80820 & 6.55701 \end{bmatrix} - \begin{bmatrix} 20.37417 & 22.19418 \\ 13.21436 & 15.71506 \end{bmatrix} \gamma^{2/3}$$

For comparison, eigenvalues of these matrices and eigenvalues found by numerical integration of the full non-linear equations are shown in Figure 3.4. Results to $O(\delta)$ were in qualitative agreement with the numerics, but the quantitative agreement is only good at very small slopes ($\gamma < 0.005$, or $\delta < 0.03$).

3.7.2 Additional Figures And Text Not Contained In The Paper

Plot of $z(\tau_0)$

A plot of Equation 3.5 is shown in Figure 3.8.

Plot Of A Multiple-Swinging Solution

Coleman (1998b) discovered these multiple-swinging motions while adjusting parameters in a slightly more complicated model. Angles over one step for one of these gait cycles are shown in Figure 3.9.
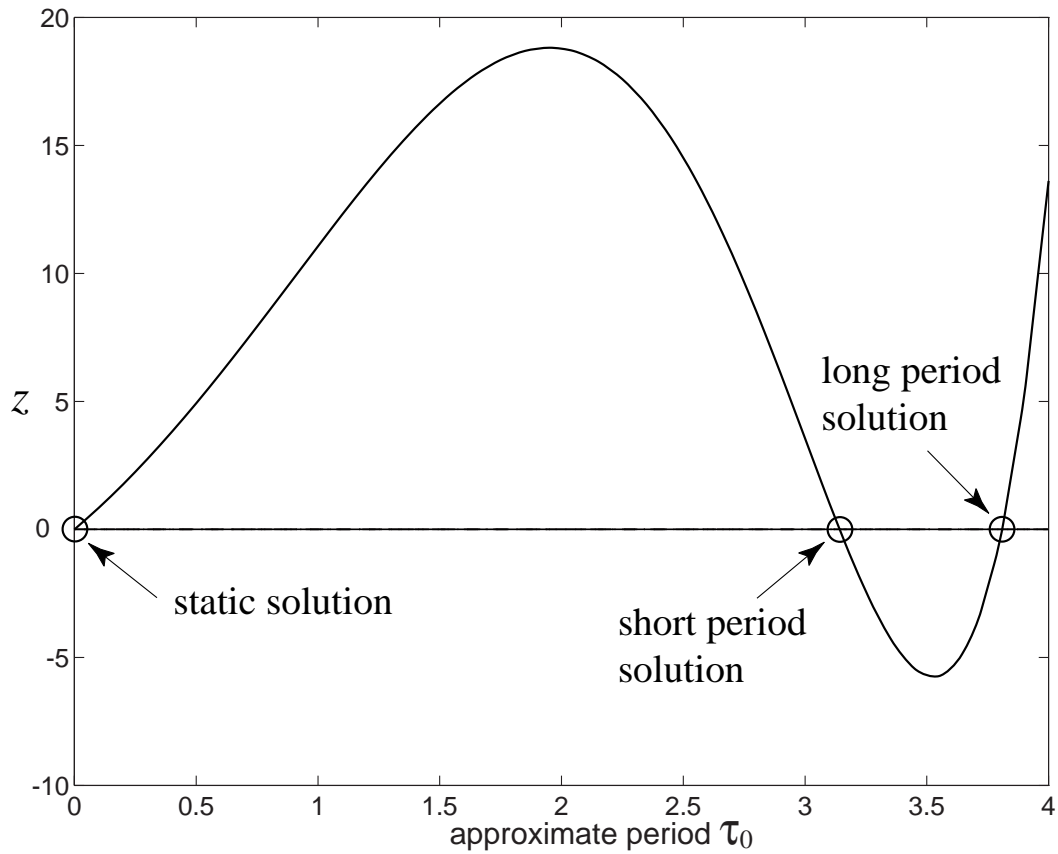
Figure 3.8: A plot of the function $z(\tau_0)$ showing locations of the zero-crossings. There are infinitely many more zero crossings for $\tau_0 > 4$ representing multiple-swinging solutions.
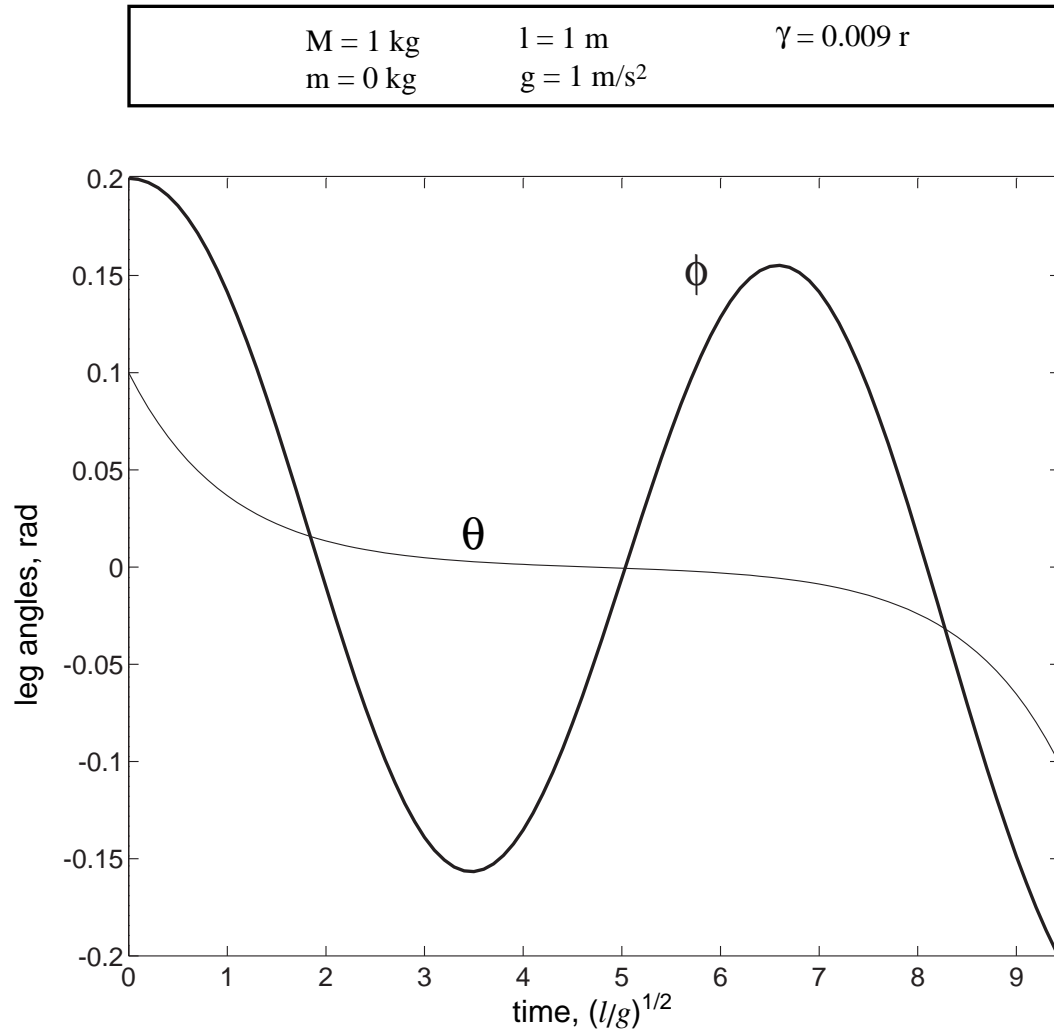
M = 1 kg	l = 1 m	γ = 0.009 r
m = 0 kg	g = 1 m/s²	

Figure 3.9: Angles vs. time for a double-swinging gait.

Step Period Comparison

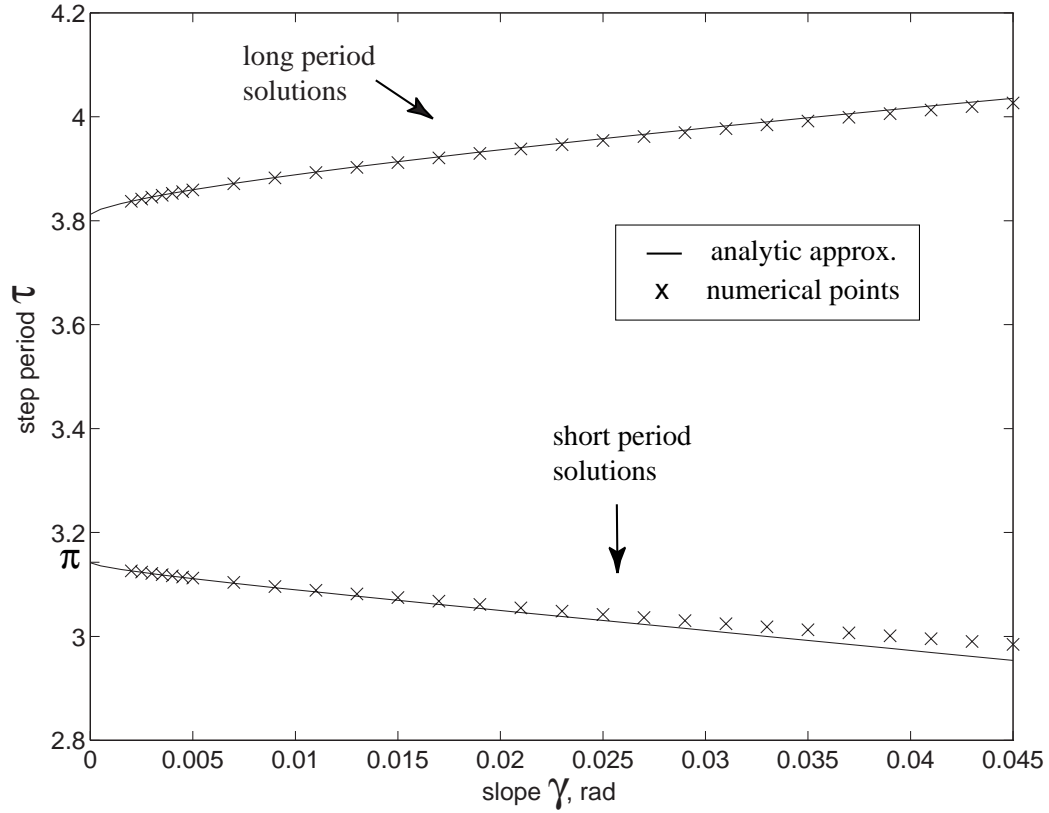In Figure 3.10 we compare analytically-predicted step periods and numerical results.

Figure 3.10: Analytically-predicted and numerically-evaluated step periods for short and long period gaits.

Return Map And Attractor

A 2D projection of the return map is shown in Figure 3.11 for $\gamma = 0.0189$. In the Poincaré section, each point represents the state of the system at the start of a step. The attractor evolves from gait cycles of increasingly higher period, as shown in Figure 3.12.

An inset of the lower portion of the attractor is shown in Figure 3.13.
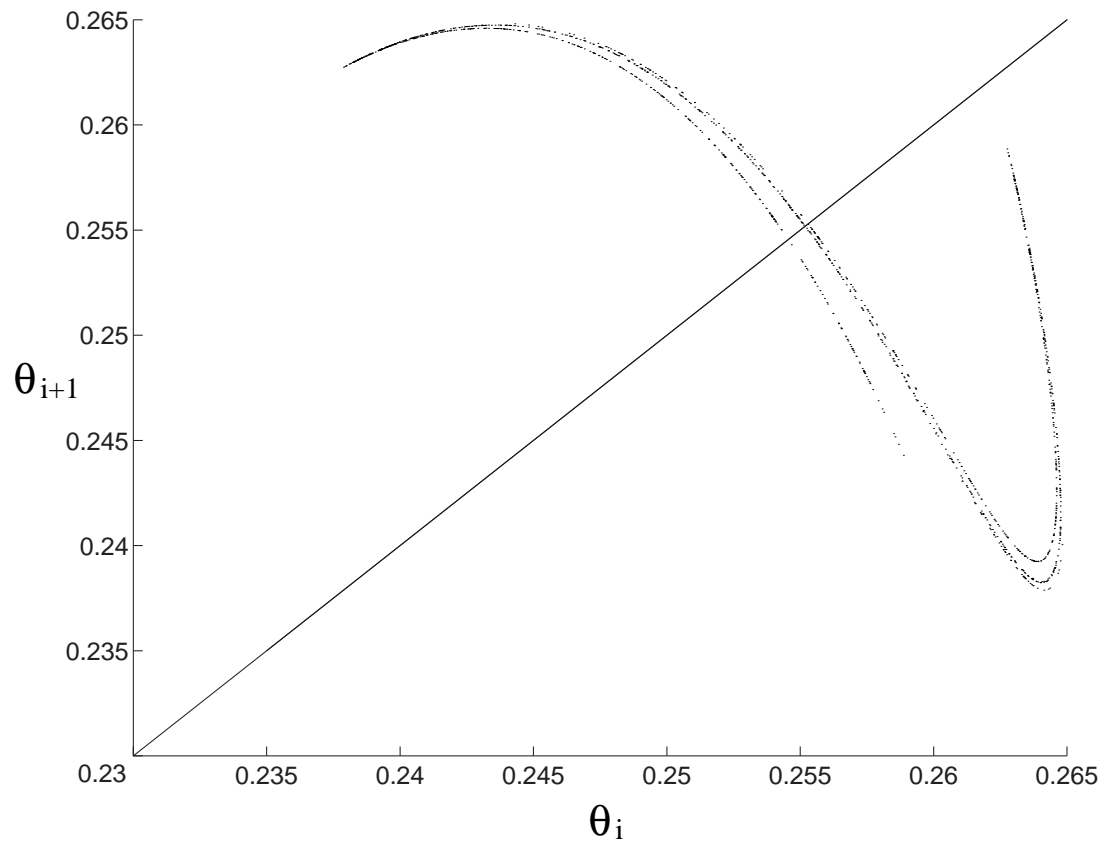
Figure 3.11: A 2D projection of the return map at $\gamma = 0.0189$. The line $\theta_i = \theta_{i+1}$ is shown for reference.
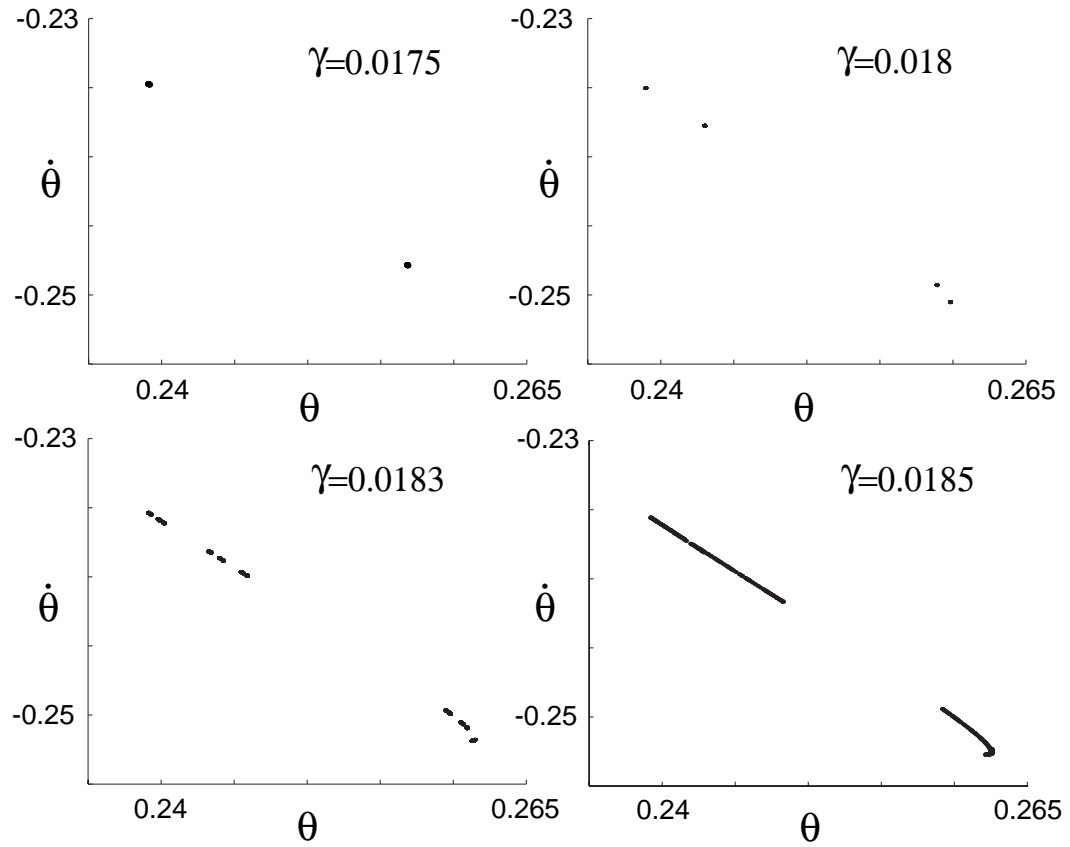
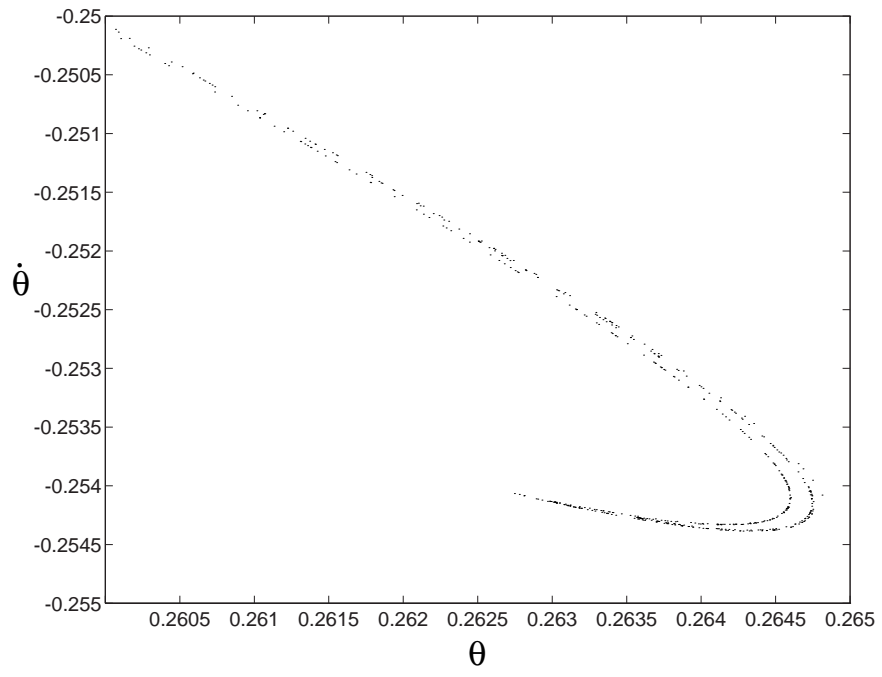Figure 3.12: Evolution of the attractor at several slopes.

Figure 3.13: Inset of lower portion of attractor showing foliated structure.